Journal of Power Sources 193 (2009) 632–638

Contents lists available at ScienceDirect

Journal of Power Sources

journal homepage: www.elsevier.com/locate/jpowsour

Developing fuel map to predict the effect of fuel composition on the maximum efficiency of solid oxide fuel cells

Siamak Farhad*, Feridun Hamdullahpur

Department of Mechanical & Aerospace Engineering, Carleton University, 1125 Colonel By Drive, Ottawa, ON K1S 5B6, Canada

ARTICLE INFO

Article history:
Received 28 February 2009
Received in revised form 18 March 2009
Accepted 19 March 2009
Available online 5 April 2009

Keywords:
Solid oxide fuel cell
Maximum cell efficiency
Fuel map
Ternary coordinate system
Fuel processor
Modeling

ABSTRACT

At any given cell operating condition, a fuel map can be developed to predict the effect of a fuel containing carbon, hydrogen, oxygen and inert gas atoms on the maximum cell efficiency (MCE) of solid oxide fuel cells (SOFCs). To create a fuel map, a thermodynamic model is developed to obtain the fuels that would yield identical MCE for SOFCs. These fuels make a continuous curve in the ternary coordinate system. A fuel map is established by developing continuous fuel curves for different MCEs at the same operating condition of a cell and representing them in the carbon–hydrogen–oxygen (C–H–O) ternary diagram. The graphical representation of fuel maps can be applied to predict the effect of the fuel composition and fuel processor on the MCE of SOFCs. As a general result, among the fuels that can be directly utilized in SOFCs, at the same temperature and pressure, the one located at the intersection of the H–C axis and the carbon deposition boundary (CDB) curve in the C–H–O ternary diagram provides the highest MCE. For any fuel that can be indirectly utilized in SOFCs, the steam reforming fuel processor always yields a higher MCE than auto-thermal reforming or partial oxidation fuel processors at the same anode inlet fuel temperature.

1. Introduction

One of the advantages of the solid oxide fuel cell (SOFC) is its ability to utilize various types of fuels, including hydrogen, carbon monoxide, hydrocarbons, alcohols and biomass. Usually, a hydrogen- and/or carbon monoxide-rich fuel that does not cause any carbon deposition over the anode catalyst can be directly utilized in SOFCs. If carbon deposition and deactivation of the anode catalyst is probable then the fuel is utilized indirectly after applying a fuel processor. Steam reforming [1–3], partial oxidation [4,5], auto-thermal reforming [6,7], and anode exit gas recirculation [8,9] are the usual methods to prepare a fuel for SOFCs. Although a broad range of fuels and fuel processors can be applied for SOFCs, their effects on the cell performance vary considerably. In this paper, the effect of any fuel containing carbon, hydrogen, oxygen and inert gas atoms on the maximum cell efficiency (MCE) of SOFCs is studied by developing fuel maps. For this purpose, a thermodynamic model is developed to identify the fuels that would yield identical MCE for SOFCs at a given cell operating condition. These fuels make a continuous curve in the ternary coordinate system. By developing the continuous fuel curves for different MCEs, at the same operating condition of a cell, and representing them in the carbon–hydrogen–oxygen (C–H–O) ternary diagram, a fuel map is established. Determination of the carbon deposition boundary (CDB) curve in the fuel map is necessary to realize a fuel can be directly utilized or it should be prepared before utilized in the SOFC. It should be noted that the region below the CDB curve in the C–H–O ternary diagram belongs to fuels that can be directly utilized in SOFCs (called “direct fuel utilization region” in this paper) and the region above the CDB curve belongs to fuels that should be processed before being utilized in SOFCs (called “indirect fuel utilization region” in this paper). The CDB curve is found based on the thermodynamic equilibrium assumption [10–13]. A simplified method to find the CDB curve for fuel maps has been presented by authors [14]. After determination of the CDB curve, the fuel map can be easily used to study the effect of any fuel containing carbon, hydrogen, oxygen and inert gas atoms on the MCE of SOFCs.

2. Model development

In the present model, all fuels located in the C–H–O ternary diagram are assumed to be in thermodynamic equilibrium and the species of primary importance of the equilibrium products of a fuel is considered in the model. At the operating temperatures and pressures of SOFCs, the species of primary importance of the equilibrium products of a fuel, located in the C–H–O ternary diagram, are carbon in solid phase and a mixture of H_2, CO, CH_4, H_2O and CO_2 in the gaseous phase [15–17]. Depending on the fuel, inert gases such as nitrogen may be present in the gaseous phase. Neglecting the amounts of the species of secondary importance in the equilibrium products of a fuel (e.g. CH_3OH, HCHO, C_2H_5OH, and $C_{10}H_{22}$) does

* Corresponding author. Tel.: +1 613 520 3806; fax: +1 613 520 2536.
E-mail addresses: sfarhad@connect.carleton.ca, siamak_farhad@yahoo.com (S. Farhad), feridun_hamdullahpur@carleton.ca (F. Hamdullahpur).

0378-7753/$ – see front matter © 2009 Elsevier B.V. All rights reserved.
doi:10.1016/j.jpowsour.2009.03.054

Nomenclature

$\dot{C}$	consumption rate (mol s^{-1})
F	Faraday constant (=96,485 C mol^{-1})
$\bar{g}$	Gibbs free energy (J mol^{-1})
$\bar{h}$	enthalpy (J mol^{-1})
I	electric current (A)
K_p	equilibrium constant
HV	heating value (J mol^{-1})
MCE	maximum cell efficiency
MCV	maximum cell voltage (V)
$\dot{n}$	molar flow rate (mol s^{-1})
p	pressure (bar)
$\dot{P}$	production rate (mol s^{-1})
R_u	universal gas constant (=8.314 J mol^{-1} K^{-1})
T	temperature (K)
U_f	fuel utilization ratio
V	voltage (V)
x	mole fraction

Greek letters

$\alpha, \beta, \gamma, \delta, \varepsilon, \psi, \omega$	defined parameters
Δ	difference
η	efficiency

Subscripts and superscripts

i	inlet
ig	inert gases
o	outlet
SR	steam reforming reaction
WGS	water gas shift reaction

not affect the results within the accuracy of the equilibrium constant data [11]. The mole fraction of species in the gaseous phase of the equilibrium product of a fuel (hereafter called just fuel) is obtained by dividing the partial pressures of H_2, CO, CH_4, H_2O, and CO_2 by the difference of the total gas pressure and the inert gases partial pressure. Using the Dalton's law[1]:

$$x_{H_2} + x_{CO} + x_{CH_4} + x_{H_2O} + x_{CO_2} = 1 \quad (1)$$

The overall cell efficiency of SOFCs is defined as the ratio of the cell electric power output to the heating value of the inlet fuel to the anode [18]. By assuming that the cell operating voltage is uniform across the cell area, the electric power output will be the product of the electric current and the operating voltage of a cell [19]. Therefore:

$$\eta = \frac{IV_{cell}}{\dot{n}_i \times HV(T_i)} \quad (2)$$

The net electric current produced in an oxygen ion conducting SOFC is related to the rate of the hydrogen consumption in the anode due to the following electrochemical reaction [20].

$$H_2 + O^{2-} \rightarrow H_2O + 2e^- \quad (R1)$$

$$I = 2F\dot{C}_{H_2} \quad (3)$$

For the inlet fuel to the anode, the heating value can be expressed as follows:

$$\dot{n}_i \times HV(T_i) = -R_u T_o(\dot{n}_i - \dot{n}_{ig,i})(x_{H_2,i}\beta + x_{CO,i}\gamma + x_{CH_4,i}\delta) \quad (4)$$

where

$$\beta = \frac{\bar{h}_{H_2O}(T_i) - \bar{h}_{H_2}(T_i) - 0.5\bar{h}_{O_2}(T_i)}{R_u T_o} \quad (5)$$

$$\gamma = \frac{\bar{h}_{CO_2}(T_i) - \bar{h}_{CO}(T_i) - 0.5\bar{h}_{O_2}(T_i)}{R_u T_o} \quad (6)$$

$$\delta = \frac{\bar{h}_{CO_2}(T_i) + 2\bar{h}_{H_2O}(T_i) - \bar{h}_{CH_4}(T_i) - 2\bar{h}_{O_2}(T_i)}{R_u T_o} \quad (7)$$

By substituting Eqs. (3) and (4) into Eq. (2), the overall cell efficiency becomes:

$$\eta = \frac{-2F}{R_u T_o}\left(\frac{\dot{C}_{H_2}}{\dot{n}_i - \dot{n}_{ig,i}}\right)\frac{V_{cell}}{(x_{H_2,i}\beta + x_{CO,i}\gamma + x_{CH_4,i}\delta)} \quad (8)$$

In Eq. (8), $\dot{C}_{H_2}/(\dot{n}_i - \dot{n}_{ig,i})$ is determined from the definition of the fuel utilization ratio [19,21,22].

$$\frac{\dot{C}_{H_2}}{(\dot{n}_i - \dot{n}_{ig,i})} = U_f\left(x_{H_2,i} + \frac{\gamma}{\beta}x_{CO,i} + \frac{\delta}{\beta}x_{CH_4,i}\right) - \left(\frac{\delta - \gamma}{\beta} - 3\right)x_{CH_4,i} - \left(\frac{\gamma}{\beta} - 1\right)\frac{\dot{P}_{CO_2}}{(\dot{n}_i - \dot{n}_{ig,i})} \quad (9)$$

where $\dot{P}_{CO_2}$ is the rate of CO_2 production by the water gas shift reaction (R2).

$$CO + H_2O \overset{K_{p,WGS}}{\longleftrightarrow} CO_2 + H_2 \quad (R2)$$

$$K_{p,WGS}(T) = \frac{x_{CO_2}x_{H_2}}{x_{CO}x_{H_2O}} \quad (10)$$

In Eq. (9), it is assumed that the methane content of the fuel is completely consumed in the anode by the steam reforming reaction (R3).

$$CH_4 + H_2O \overset{K_{p,SR}}{\longleftrightarrow} CO + 3H_2 \quad (R3)$$

$$K_{p,SR}(T) = \frac{x_{CO}x_{H_2}^3(p - p_{ig})^2}{x_{CH_4}x_{H_2O}} \quad (11)$$

By developing Eq. (10) for the anode outlet fuel that is assumed to be in thermodynamic equilibrium, depending on the equilibrium constant of reaction (R2) at the temperature of the anode outlet fuel, $\dot{P}_{CO_2}/(\dot{n}_i - \dot{n}_{ig,i})$ is obtained as Eq. (12)

$$\frac{\dot{P}_{CO_2}}{(\dot{n}_i - \dot{n}_{ig,i})} = \frac{-\left[(x_{CO,i} + x_{CH_4,i})\left(x_{CH_4,i}\left(\frac{\delta - \gamma}{\beta} - 2\right) - x_{H_2O,i} - U_f\left(x_{H_2,i} + \frac{\gamma}{\beta}x_{CO,i} + \frac{\delta}{\beta}x_{CH_4,i}\right)\right) + x_{CO_2,i}\left(x_{H_2,i} + x_{CH_4,i}\left(\frac{\delta - \gamma}{\beta}\right) - U_f\left(x_{H_2,i} + \frac{\gamma}{\beta}x_{CO,i} + \frac{\delta}{\beta}x_{CH_4,i}\right)\right)\right]}{\left[2x_{CH_4,i} + \left(\frac{\gamma}{\beta} - 1\right)(x_{CO_2,i} + x_{CO,i} + x_{CH_4,i}) + 1\right]}$$

$$(K_{p,WGS}(T_o) = 1)$$

$$\frac{\dot{P}_{CO_2}}{(\dot{n}_i - \dot{n}_{ig,i})} = -\frac{\psi}{2} - \sqrt{\left(\frac{\psi}{2}\right)^2 - \omega} \quad (K_{p,WGS}(T_o) > 1)$$

$$\frac{\dot{P}_{CO_2}}{(\dot{n}_i - \dot{n}_{ig,i})} = -\frac{\psi}{2} + \sqrt{\left(\frac{\psi}{2}\right)^2 - \omega} \quad (K_{p,WGS}(T_o) < 1) \quad (12)$$

[1] See Nomenclature.

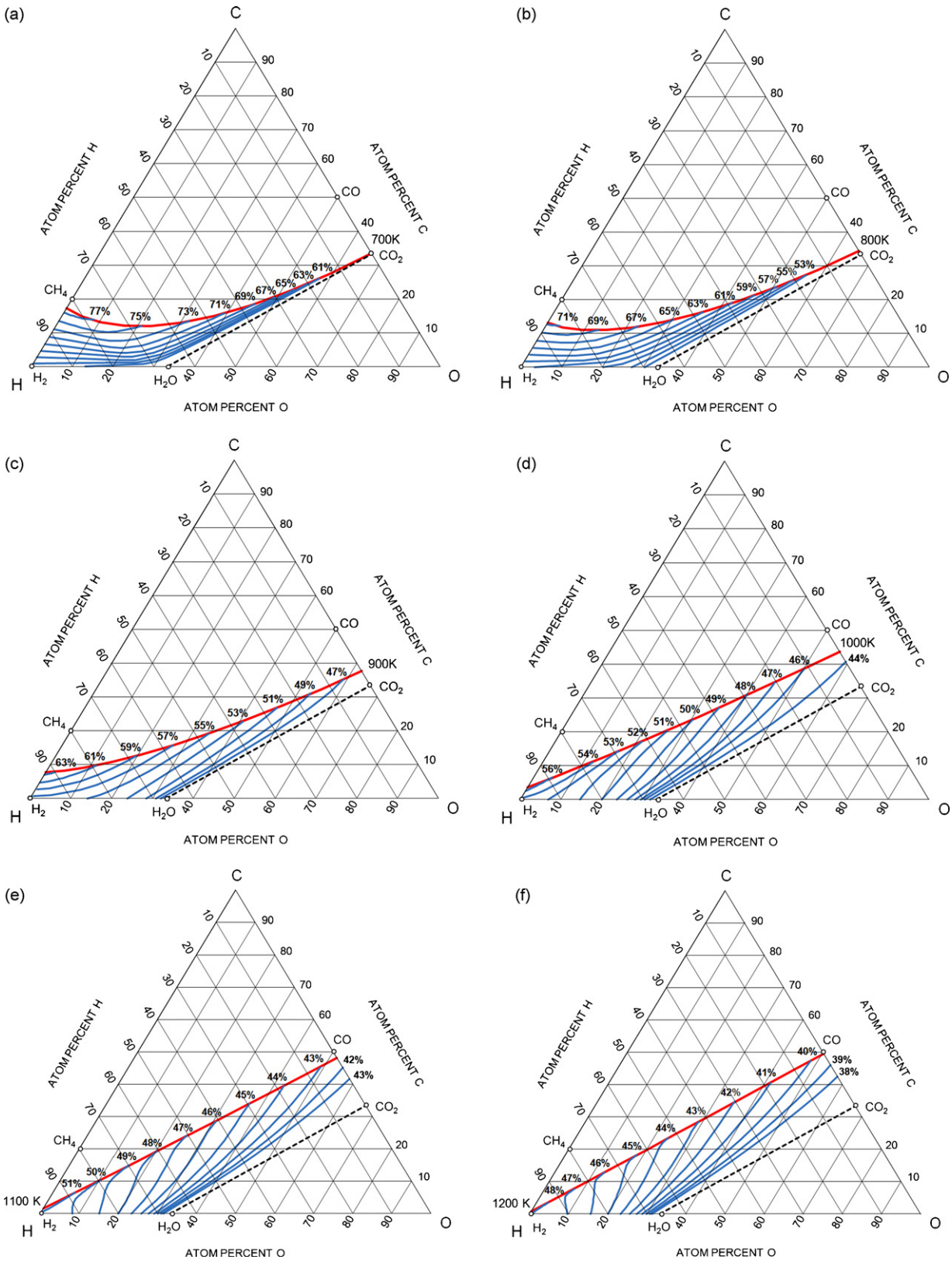

Fig. 1. Fuel map for MCE of SOFCs at $p = 1$ atm, $U_f = 0.85$, $\Delta T = 200$ K, $x_{O_2} = 0.21$, $p_{ig} = 0$ and (a) $T_i = 700$ K, (b) $T_i = 800$ K, (c) $T_i = 900$ K, (d) $T_i = 1000$ K, (e) $T_i = 1100$ K, and (f) $T_i = 1200$ K (continuous fuel curves are blue and CDB curves are red). (For interpretation of the references to color in this figure legend, the reader is referred to the web version of the article.)

where

$$\psi = \frac{\beta}{\gamma}\left[x_{H_2,i} + x_{CO_2,i} + x_{CH_4,i} - U_f\left(x_{H_2,i} + \frac{\gamma}{\beta}x_{CO,i} + \frac{\delta}{\beta}x_{CH_4,i}\right) + \left(\frac{\delta-\gamma}{\beta} - 3\right)x_{CH_4,i} + \frac{2x_{CH_4,i} + \left(\frac{\gamma}{\beta}-1\right)x_{CO_2,i} + K_{p,WGS}(T_o)\left(1 + \left(\frac{\gamma}{\beta}-1\right)(x_{CO,i} + x_{CH_4,i})\right)}{1 - K_{p,WGS}(T_o)}\right] \quad (13)$$

$$\omega = \frac{\beta}{\gamma(1-K_{p,WGS}(T_o))}\left[K_{p,WGS}(T_o)(x_{CO,i} + x_{CH_4,i})\left(x_{CH_4,i}\left(\frac{\delta-\gamma}{\beta} - 2\right) - x_{H_2O,i} - U_f\left(x_{H_2,i} + \frac{\gamma}{\beta}x_{CO,i} + \frac{\delta}{\beta}x_{CH_4,i}\right)\right) + x_{CO_2,i}\left(x_{H_2,i} + x_{CH_4,i}\left(\frac{\delta-\lambda}{\beta}\right) - U_f\left(x_{H_2,i} + \frac{\gamma}{\beta}x_{CO,i} + \frac{\delta}{\beta}x_{CH_4,i}\right)\right)\right] \quad (14)$$

According to Eqs. (9) and (12), at the fixed inlet fuel composition and temperature to the anode; the fuel utilization ratio; and the outlet fuel temperature from the anode, the overall cell efficiency is a function of the cell operating voltage. In this condition, the overall cell efficiency is maximized once the cell operating voltage is maximized. If it is assumed that the fuel utilization ratio is sufficiently high so that the minimum local Nernst voltage and the maximum local internal resistance in a cell take place at the end of the anode (the last point in the anode, along the fuel channel, that electrochemical reactions take place), the maximum voltage that a cell can achieve is limited to the local Nernst voltage at the end of the anode [14]. Therefore, the maximum cell voltage (MCV) is obtained as follows:

$$MCV = \frac{-R_u T_o}{2F}(\alpha + \ln(\varepsilon)) \quad (15)$$

where

$$\alpha = \frac{\bar{g}^0_{H_2O}(T_o) - \bar{g}^0_{H_2}(T_o) - 0.5\bar{g}^0_{O_2}(T_o)}{R_u T_o} - 0.5\ln(x_{O_2}p) \quad (16)$$

$$\varepsilon = \frac{x_{H_2O,o}}{x_{H_2,o}} = \frac{x_{H_2O,i} - x_{CH_4,i} - (\dot{P}_{CO_2}/\dot{n}_i - \dot{n}_{ig,i}) + (\dot{C}_{H_2}/\dot{n}_i - \dot{n}_{ig,i})}{x_{H_2,i} + 3x_{CH_4,i} + (\dot{P}_{CO_2}/\dot{n}_i - \dot{n}_{ig,i}) - (\dot{C}_{H_2}/\dot{n}_i - \dot{n}_{ig,i})} \quad (17)$$

By substituting Eq. (15) into Eq. (8), the MCE of SOFCs will be:

$$MCE = \left(\frac{\dot{C}_{H_2}}{\dot{n}_i - \dot{n}_{ig,i}}\right)\left(\frac{\alpha + \ln(\varepsilon)}{x_{H_2,i}\beta + x_{CO,i}\gamma + x_{CH_4,i}\delta}\right) \quad (18)$$

According to Eq. (18), at the given cell operating condition of the anode inlet and outlet fuel temperatures; the cell operating pressure; the oxygen mole fraction at the cathode; and the fuel utilization ratio, the MCE depends only on the fuel composition at the anode inlet.

Now, at a fixed operating condition of a cell, the composition of fuels that yield identical MCE for oxygen ion conducting SOFCs is determined. By solving Eqs. (1), (10) and (11) for the anode inlet fuel, $x_{CO_2,i}$, $x_{CO,i}$, and $x_{CH_4,i}$ are obtained as follows:

$$x_{CO_2 i} = \frac{K_{p,WGS}(T_i)x^2_{H_2O,i}(1 - x_{H_2O,i} - x_{H_2,i})}{K_{p,WGS}(T_i)x^2_{H_2O,i} + x_{H_2,i}x_{H_2O,i} + (x^4_{H_2,i}(p - p_{ig})^2/K_{p,SR}(T_i))} \quad (19)$$

$$x_{CO,i} = \frac{x_{H_2,i}x_{H_2O,i}(1 - x_{H_2O,i} - x_{H_2,i})}{K_{p,WGS}(T_i)x^2_{H_2O,i} + x_{H_2}x_{H_2O,i} + (x^4_{H_2,i}(p - p_{ig})^2/K_{p,SR}(T_i))} \quad (20)$$

$$x_{CH_4,i} = \frac{(x^4_{H_2,i}(p - p_{ig})^2/K_{p,SR}(T_i))(1 - x_{H_2O,i} - x_{H_2,i})}{K_{p,WGS}(T_i)x^2_{H_2O,i} + x_{H_2,i}x_{H_2O,i} + (x^4_{H_2,i}(p - p_{ig})^2/K_{p,SR}(T_i))} \quad (21)$$

For a specified MCE, an equation to obtain $x_{H_2O,i}$ is found from Eq. (18):

$$x_{H_2O,i} = 1 - x_{CO_2,i} + \left(\frac{\gamma}{\beta} - 1\right)x_{CO,i} + \left(\frac{\delta}{\beta} - 1\right)x_{CH_4,i} - \frac{1}{\beta}\left(\frac{\dot{C}_{H_2}}{\dot{n}_i - \dot{n}_{ig,i}}\right)\left(\frac{\alpha + \ln(\varepsilon)}{MCE}\right) \quad (22)$$

By varying $x_{H_2,i}$ from 0 to 1 in Eqs. (19)–(22), the composition of fuels that yield identical MCE at a given cell operating condition is determined. Among these fuels, those located below the CDB curve in the C–H–O ternary diagram can be directly utilized in the anode. These fuels make a continuous curve in the ternary coordinate system. A fuel map is established by developing continuous fuel curves for different MCEs at the same operating condition of a cell and representing them in the C–H–O ternary diagram.

3. Results

The predictions obtained from the current model for some fuels that yield the MCE of 59% are shown in Table 1 for the anode inlet and outlet fuel temperatures of $T_i = 900$ K and $T_o = 1100$ K, respectively ($\Delta T = T_o - T_i = 200$ K); the cell operating pressure of $p = 1$ atm; the fuel utilization ratio of $U_f = 0.85$; and the oxygen mole fraction of $x_{O_2} = 0.21$. According to this table, the presence of methane in the inlet fuel does not necessarily lead to an increase in the MCE of SOFCs.

In Fig. 1, fuel maps to predict the effect of a fuel on the MCE are shown at different inlet fuel temperatures of 700 K, 800 K, 900 K, 1000 K, 1100 K, and 1200 K at the cell operating condition of $p = 1$ atm, $U_f = 0.85$, $\Delta T = 200$ K, $x_{O_2} = 0.21$, and $p_{ig} = 0$. In this figure, blue curves are the continuous fuel curves and red curves are the CDB curves. As can be clearly seen in this figure, the fuel com-

Table 1
The composition of the anode inlet fuels that yield MCE = 59% at $T_i = 900$ K, $\Delta T = T_o - T_i = 200$ K, $p = 1$ atm, $U_f = 0.85$, and $x_{O_2} = 0.21$.

No.	Mole fraction (%)				
	x_{CH_4}	x_{H_2}	x_{CO}	x_{H_2O}	x_{CO_2}
1	5.7	90.6	0.3	3.4	0.0
2	6.0	83.5	1.2	9.0	0.3
3	6.3	77.4	2.3	13.1	0.9
4	6.6	72.1	3.6	15.9	1.8
5	7.0	66.3	5.5	17.8	3.4
6	7.3	62.6	7.0	18.4	4.7
7	7.6	59.3	8.6	18.4	6.1
8	8.0	55.5	10.7	17.9	7.9
9	8.2	53.7	11.8	17.5	8.8
10	8.4	52.3	12.8	17.0	9.5

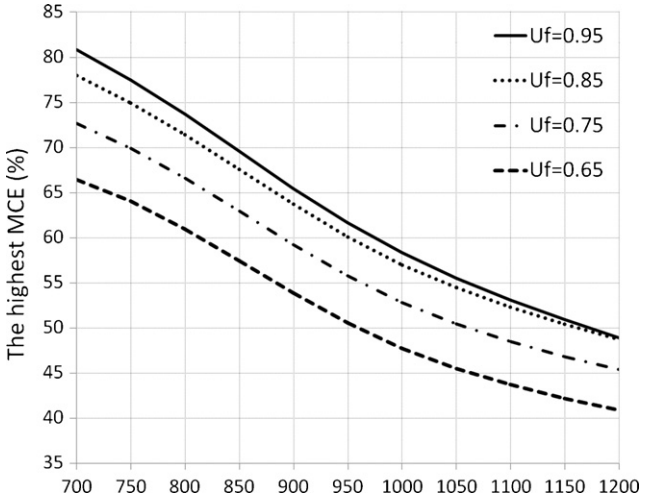

Fig. 2. Effect of the anode inlet fuel temperature on the highest MCE at different fuel utilization ratios and at $p = 1$ atm, $\Delta T = T_o - T_i = 200$ K, $x_{O_2} = 0.21$, $x_{ig} = 0$.

position has a significant effect on the MCE. The following general results can be obtained for the fuels in the direct and indirect fuel utilization regions in the C–H–O ternary diagram.

3.1. Direct fuel utilization region

This region is below the CDB curve (red curve) in fuel maps. In this region, for the anode inlet fuel temperatures greater than 800 K, among the fuels with the same percentage of carbon atoms, the one with a higher percentage of hydrogen atom yields a higher MCE at a given operating condition of a cell. At lower inlet fuel temperatures, for example 700 K, the MCE is not necessarily higher for a fuel that contains a higher atomic percentage of hydrogen.

For anode inlet temperatures between 800 K and 1100 K, if a fuel is located either below or at the right of another fuel in the fuel map, it yields a lower MCE. This result cannot be generalized for the inlet fuel temperatures of less than 800 K or more than 1100 K.

In many cases, the MCE can be increased by mixing a fuel located in the direct fuel utilization region with a fuel located in the indirect fuel utilization region in a fuel map. For example, if a fuel located at C = 17.7% and H = 50.6% is mixed with natural gas ($x_{CH_4} = 88.5\%$, $x_{C_2H_6} = 4.8\%$, $x_{C_3H_8} = 1.6\%$, $x_{C_4H_{10}} = 0.7\%$, and $x_{N_2} = 4.4\%$ [23]), according to Fig. 1e, the MCE increases up to around 2.3%. In certain cases, adding CO or even CO_2 to a fuel may lead to an increase in the MCE. For example, at the inlet fuel temperature of 800 K (Fig. 1b), adding CO to a fuel located at C = 2% and H = 98% can increase the MCE up to around 8%. Adding CO_2 also increases the MCE up to around 6% for this case, while adding H_2, H_2O, or O_2 result in reduced MCE.

Among fuels that are at the same temperature and pressure, the highest SOFC MCE is given by the one located at the intersection of the CDB curve and the H–C axis in the fuel map. This fuel contains only H_2 and CH_4; however, a small quantity of water vapour should be added to start the electrochemical reaction at the anode. The location of this fuel depends on the anode inlet fuel temperature and pressure. At the inlet fuel temperatures of more than 1200 K and the cell operating pressures of the order of 1 atm, almost pure hydrogen is the fuel that yields the highest MCE for SOFCs. The effect of the inlet fuel temperature on the highest MCE at different fuel utilization ratios and fuel temperature rises along the anode ($\Delta T = T_o - T_i$) are illustrated in Figs. 2 and 3, respectively. According to these figures, for each 100 K increase in the anode inlet fuel temperature, the highest MCE reduces $5.6 \pm 2.6\%$ depending on the fuel utilization ratio. Increasing the fuel utilization ratio and decreasing $\Delta T = T_o - T_i$ lead to an increase in the highest MCE at the same anode inlet fuel temperature.

3.2. Indirect fuel utilization region

This region is above the CDB curve (red curve) in fuel maps. In this region, the composition of fuel and the type of fuel processor affect the MCE of SOFCs. Among the fuels with the same percentage of carbon atom, a fuel with a higher percentage of hydrogen atom yields a higher MCE at the given operating condition of a cell, regardless of the type of fuel processor.

We decided to use an example to explain the effect of different types of fuel processors on the MCE. In this example, CH_4 (C = 20% and H = 80%) at 900 K is used in a cell that operates at $p = 1$ atm, $U_f = 0.85$, $\Delta T = 200$ K, and $x_{O_2} = 0.21$. This fuel is in the indirect fuel utilization region and should be processed before it can be utilized in the anode. If partial oxidation is selected as the fuel processor, according to Fig. 1c, at least 0.86 mol of O_2 should be added to each mole of CH_4 to cross the CDB curve which will then result in an MCE value around 57.4%. If steam reforming is selected as a fuel processor, at least 1.4 mol of H_2O should be added to each mole of CH_4 and the MCE will be around 60.1%. For the auto-thermal reforming fuel processor, depending on how much H_2O and O_2 are added to the fuel, the MCE varies between 57.4% and 60.1%. The dry reforming of CH_4 is also possible by adding almost 6.7 mol of CO_2 to each mole of CH_4; however the MCE reaches around 49%. If 4 mol of H_2 are added to each mole of CH_4 at 900 K, the MCE corresponding to the new mixture will be around 63%. Another method is to separate the solid phase carbon from the equilibrium product of CH_4. By separating the solid carbon, the location of the fuel moves toward the CDB curve along a line that connects the fuel to the C vertex in the fuel map. For this method the MCE will be about 63%. The effect of the anode exit gas recirculation on the MCE is always the same as the partial oxidation fuel processor. As a general result, for any fuel in the indirect fuel utilization region, the steam reforming fuel processor yields a higher MCE than partial oxidation or auto-thermal reforming fuel processors at a specific operating condition of a cell.

3.3. Effect of the cell operating condition

To predict the effect of the cell operating condition on the location of continuous fuel curves (blue curves) in fuel maps, a parametric study is performed and the results are shown in Fig. 4. According to Fig. 4a, by decreasing the anode inlet fuel tempera-

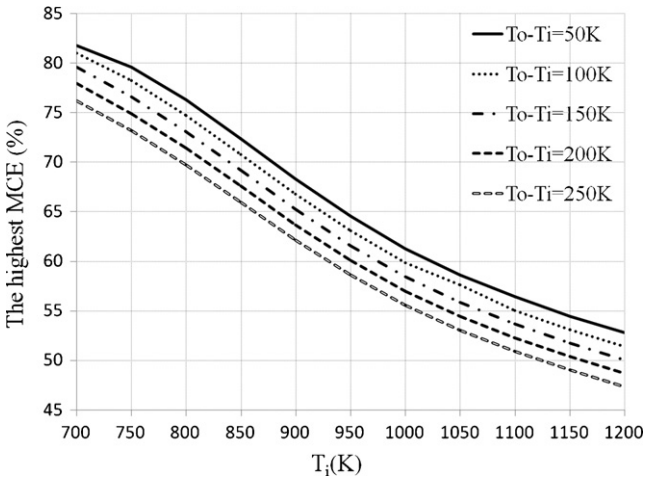

Fig. 3. Effect of the anode inlet fuel temperature on the highest MCE at different fuel temperature rise along the anode ($\Delta T = T_o - T_i$) and at $p = 1$ atm, $U_f = 0.85$, $x_{O_2} = 0.21$.

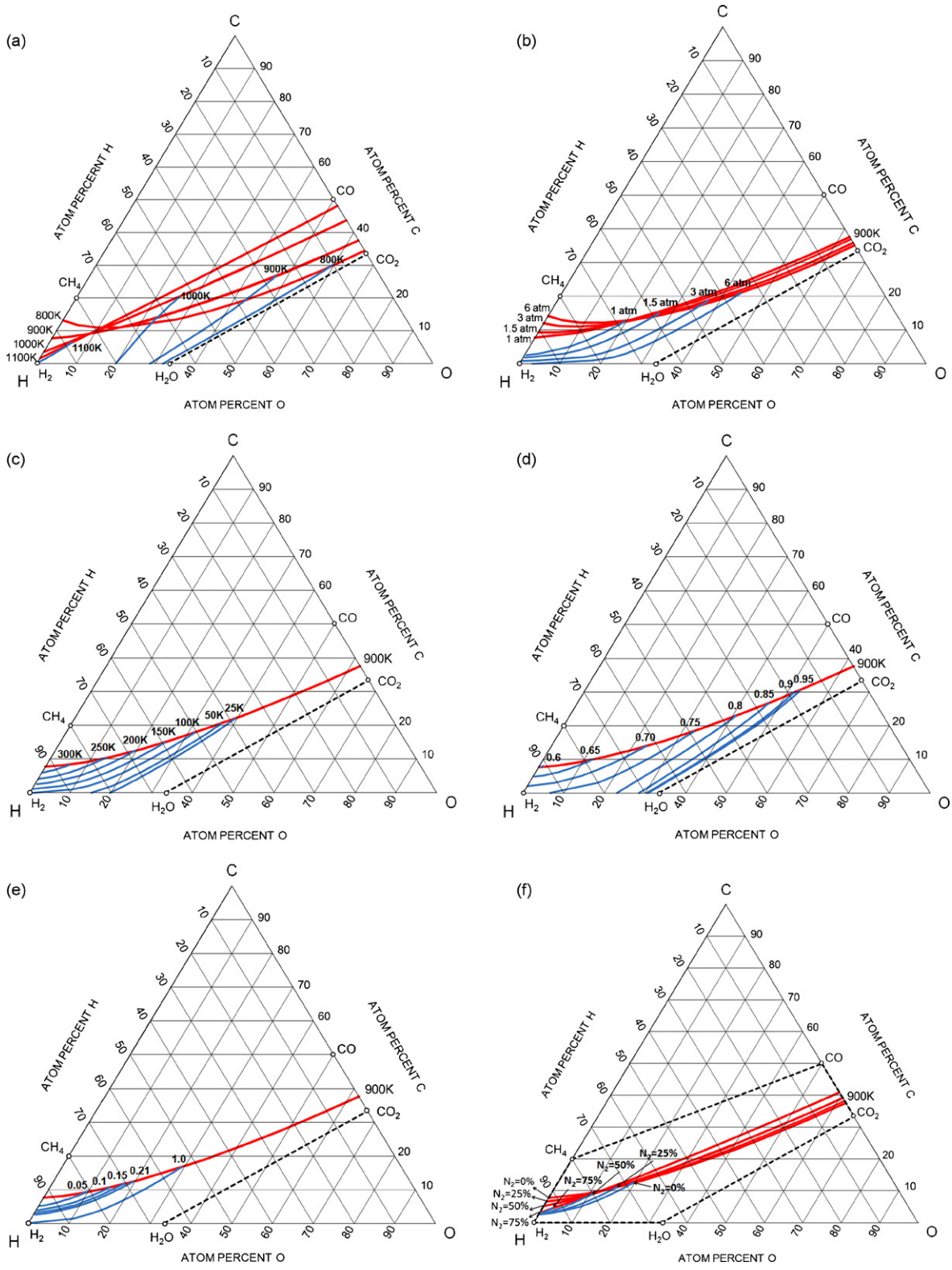

Fig. 4. Effect of the (a) anode inlet fuel temperature, (b) cell operating pressure, (c) fuel temperature rise along the anode, (d) fuel utilization ratio, (e) oxygen mole fraction in cathode, and (f) nitrogen (or any other inert gas) mole fraction, on the location of continuous fuel curves in fuel maps (continuous fuel curves are blue and CDB curves are red). (For interpretation of the references to color in this figure legend, the reader is referred to the web version of the article.)

[f.]

a. MCE = 51%, p = 1 atm, U_f = 0.85, ΔT = 200 K, $x_{O_2} = 0.21$, p_{ig} = 0.
b. MCE = 59%, T_i = 900 K, U_f = 0.85, ΔT = 200 K, $x_{O_2} = 0.21$, p_{ig} = 0.
c. MCE = 59%, T_i = 900 K, p = 1 atm, U_f = 0.85, $x_{O_2} = 0.21$, p_{ig} = 0.
d. MCE = 51%, T_i = 900 K, p = 1 atm, ΔT = 200 K, $x_{O_2} = 0.21$, p_{ig} = 0.
e. MCE = 59%, T_i = 900 K, p = 1 atm, U_f = 0.85, ΔT = 200 K, p_{ig} = 0.
f. MCE = 59%, T_i = 900 K, p = 1 atm, U_f = 0.85, ΔT = 200 K, $x_{O_2} = 0.21$.

ture, the continuous fuel curves corresponding to an MCE shift to the right of fuel maps. This means, the fuels with a lower hydrogen atom percentage (with the same percentage of carbon atom) may still yield a high MCE if the anode inlet fuel temperature is reduced. According to Fig. 4b, d, and e, by increasing the cell operating pressure, the fuel utilization ratio, or oxygen mole fraction in cathode, the continuous fuel curves tend to move to the right of the fuel maps. As observed in Fig. 4c and f, the continuous fuel curves shift to the right of fuel maps by decreasing either the fuel temperature rise along the anode ($\Delta T = T_o - T_i$) or the inert gases mole fraction.

4. Conclusions

At the given cell operating condition of the anode inlet and outlet fuel temperatures; cell operating pressure; oxygen mole fraction at cathode; and the fuel utilization ratio; the MCE of oxygen ion conducting SOFCs depends only on the inlet fuel composition to the anode. To predict the effect of the composition of any fuel containing carbon, hydrogen, oxygen, and inert gas atoms on the MCE of SOFCs, a thermodynamic model is developed to create a fuel map at the specified operating condition of a cell. According to fuel maps, the composition of a fuel has a significant effect on the MCE of SOFCs. Fuel maps are also useful for selecting an appropriate fuel processor for a fuel that cannot be directly utilized in SOFCs due to the carbon deposition problem.

Some of the general results obtained from fuel maps are presented as follows:

- In the direct fuel utilization region, for the anode inlet fuel temperatures greater than 800 K, among the fuels with the same percentage of carbon atom, the one with a higher percentage of hydrogen atom yields a higher MCE at a given operating condition of a cell. This result is also valid for fuels in the indirect fuel utilization region, regardless of the anode inlet fuel temperature and the type of fuel processor.
- In the direct fuel utilization region, for the anode inlet fuel temperatures between 800 K and 1100 K, if a fuel is located either below or at the right of another fuel in the fuel map, it yields a lower MCE.
- In the direct fuel utilization region, adding CO or even CO_2 to a fuel sometimes increases the MCE.
- In many cases, the MCE can be increased by mixing a fuel located at the direct fuel utilization region with a fuel located at the indirect fuel utilization region in a fuel map.
- Among fuels which are at the same temperature and pressure in the direct fuel utilization region, the highest MCE always yields by a fuel located at the intersection of the CDB curve and the H–C axis in the fuel map.
- For any fuel in the indirect fuel utilization region, the steam reforming fuel processor yields a higher MCE than partial oxidation and auto-thermal reforming fuel processors at a given operating condition of a cell.
- By decreasing the anode inlet fuel temperature, the fuel temperature rise along the anode ($\Delta T = T_o - T_i$), or the inert gases mole fraction, the continuous fuel curves corresponding to an MCE shift to the right of fuel maps.
- By increasing the fuel utilization ratio, the cell operating pressure, or the oxygen mole fraction in cathode, the continuous fuel curves corresponding to an MCE shift to the right of fuel maps.

Acknowledgement

The authors gratefully acknowledge financial supports provided by the Natural Sciences and Engineering Research Council of Canada (NSERC).

References

[1] L.E. Arteaga, L.M. Peralta, V. Kafarov, Y. Casas, E. Gonzales, Chem. Eng. J. 136 (2008) 256–266.
[2] R.J. Braun, S.A. Kleina, D.T. Reindla, J. Power Sources 158 (2) (2006) 1290–1305.
[3] S.H. Chan, O.L. Ding, Int. J. Hydrogen Energy 30 (2005) 167–179.
[4] P. Piroonlerkgul, S. Assabumrungrat, N. Laosiripojana, A.A. Adesina, Chem. Eng. J. 140 (2008) 341–351.
[5] N. Hotz, S.M. Senn, D. Poulikakos, J. Power Sources 158 (2006) 333–347.
[6] A. Franzoni, L. Magistri, A. Traverso, A.F. Massardo, Energy 33 (2008) 311–320.
[7] V. Modafferi, G. Panzera, V. Baglio, F. Frusteri, P.L. Antonucci, Appl. Catal. A: Gen. 334 (2008) 1–9.
[8] C.O. Colpan, I. Dincer, F. Hamdullahpur, Int. J. Hydrogen Energy 32 (2007) 787–795.
[9] R. Peters, E. Riensche, P. Cremer, J. Power Sources 86 (2000) 432–441.
[10] V. Alderucci, P.L. Antonucci, G. Maggio, N. Giordano, V. Antonucci, Int. J. Hydrogen Energy 19 (4) (1994) 369–376.
[11] S. Assabumrungrat, N. Laosiripojana, V. Pavarajarn, W. Sangtongkitcharoen, A. Tangjitmatee, P. Praserthdam, J. Power Sources 139 (2005) 55–60.
[12] W. Sangtongkitcharoen, S. Assabumrungrat, V. Pavarajarn, N. Laosiripojana, P. Praserthdam, J. Power Sources 142 (2005) 75–80.
[13] J. Koh, B. Kang, C.H. Lim, Y. Yoo, Electrochem. Solid-State Lett. 4 (2) (2001) A12–A15.
[14] S. Farhad, F. Hamdullahpur, J. Power Sources, 2009, doi:10.1016/j.jpowsour.2009.02.073.
[15] E.J. Cairns, A.D. Tevebaugh, J. Chem. Eng. Data 9 (3) (1964) 453–462.
[16] G.H.J. Broers, B.W. Treijte, Adv. Energy Conv. 5 (1965) 365–382.
[17] K. Sasaki, Y. Teraoka, J. Electrochem. Soc. 150 (7) (2003) A878–A884.
[18] C.O. Colpan, I. Dincer, F. Hamdullahpur, Int. J. Energy Res. 32 (2008) 336–355.
[19] H. Zhu, R.J. Kee, J. Power Sources 161 (2006) 957–964.
[20] P.W. Li, M.K. Chyu, J. Power Sources 124 (2003) 487–498.
[21] B. Thorstensen, J. Power Sources 92 (2001) 9–16.
[22] Y. Hao, D.G. Goodwin, J. Power Sources 183 (2008) 157–163.
[23] S. Farhad, M. Younessi-Sinaki, M.R. Golriz, F. Hamdullahpur, Int. J. Exergy 5 (2) (2008) 164–176.